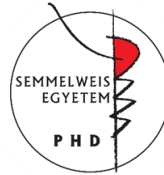


MULTIMODAL SKIN IMAGING ASSESSMENT OF RARE, INHERITED DISORDERS

PhD thesis

Pálma Anker, MD

Semmelweis University
Károly Rácz Doctoral School of Clinical Medicine



Supervisor: Márta Medvecz MD, PhD

Official reviewers: Péter Reismann MD, PhD, med.
habil., Eszter Szlávicz MD, PhD

Head of the Complex Examination Committee:
Prof. Miklós Csala, MD, PhD, DSc

Members of the Complex Examination Committee:
Barbara Molnár-Érsek, PhD, Eszter Baltás, MD, PhD

Budapest
2023

1. INTRODUCTION

Genodermatoses comprise a large group of rare, inherited diseases with cutaneous manifestations. While some diseases affect only the skin, such as non-syndromic ichthyoses, others like Fabry disease (FD) may present with multisystemic involvement. Although, notable advancements have been made in improving the diagnostic methods for genodermatoses, there remains a strong interest in understanding the optical changes in the skin in these conditions. As the therapeutic modalities develop, following the optical changes of the skin with different imaging modalities can be a convenient way for treatment monitoring.

Multispectral imaging (MSI) refers to a novel non-invasive, *in vivo* technology that captures images using a combination of multiple LED lights with different wavelengths. By using various wavelengths, the technique can be used to determine the distribution of the endogenous fluorophores of the skin such as keratin, melanin and hemoglobin.

Nonlinear microscopy (NLM) holds great promise as a label-free imaging technique. To achieve the generation of nonlinear optical processes, a high photon density is necessary, which can be attained through femtosecond or picosecond pulse laser systems operating within the near-infrared spectrum. While excitation occurs in the near-infrared wavelength range, the emitted photons fall within the visible light spectrum. Two-photon absorption fluorescence (TPF) enables the visualization of keratins, elastin, and melanin, whereas second-harmonic generation (SHG) is employed for the imaging of non-centrosymmetric molecules, such as collagen.

2. OBJECTIVES

Our objective was to apply MSI and nonlinear microscopy in a case of epidermolytic ichthyosis (EI) and for the assessment of angiokeratomas in a cohort of FD patients. Besides imaging, we also aimed to examine the clinical and dermoscopic morphologic features of angiokeratomas and other cutaneous signs in our FD patient cohort.

Our first aim was to investigate the use of MSI in keratinization disorders with the focus on a rare KPI caused by a *KRT1* gene mutation. We evaluated MSI in detecting and visualizing optical changes in the skin in case of EI.

We aimed to utilize *ex vivo* NLM modalities with particular focus on the visualization of alterations brought on by hyperkeratosis.

We assessed the utility of MSI for evaluating angiokeratomas in FD patients. Our aim was to capture autofluorescence and diffuse reflectance images of angiokeratomas and compare the images to dermoscopy to determine whether MSI provides additional information.

We explored the application of *ex vivo* NLM for distinguishing angiokeratomas from other vascular lesions such as hemangiomas.

We characterized the clinical and morphologic features of angiokeratomas in patients with FD. Our objective was to examine the distribution, appearance, and variability of angiokeratomas in FD. This involved

conducting a thorough dermatological examination, evaluating dermoscopic images, and describing the specific structures observed in angiokeratomas.

We investigated the diagnostic challenges and heterogeneity of dermatological manifestations in FD. Our aim was to explore the clinical heterogeneity of FD in our patient cohort and its impact on the diagnosis of the condition. We analyzed the distribution and appearance of angiokeratomas. Additionally, we evaluated other cutaneous signs of FD.

3. METHODS

3.1. Assessment of an epidermolytic ichthyosis case with MSI and NLM

We conducted this assessment of the skin lesions in a 3-year-old male patient with EI using *in vivo* MSI and *ex vivo* NLM to specifically investigate and visualize the changes associated with hyperkeratosis. For the confirmation of the diagnosis, genetical analysis was carried out. The genomic DNA was extracted from peripheral blood leukocytes obtained from the patient as well as his parents. The amplification of exons and

adjacent intron regions was carried out using predetermined *KRT1*-specific primers that were tagged with M13 tail sequences. This amplification process was conducted using the VariantSEQR PCR sequencing system (Applied Biosystems, Foster City, CA, USA). For *in vivo* MSI imaging, an experimental LED-based device was employed. Autofluorescence images were captured under continuous excitation of a 405 nm LED, diffuse reflectance images were obtained using 526 nm illumination. To ensure consistent illumination and a fixed distance of 60 mm between the camera and the uniformly lit skin, a cylindrical light-shielding wall was utilized, which housed four battery-powered violet and green LEDs. A long pass filter (>515 nm) was positioned in front of a color CMOS 5-megapixel IDS camera (MT9P006STC, IDS uEye UI3581LE-C-HQ, Obersulm, Germany) to prevent the detection of 405 nm LED emissions. The skin of the patient was evaluated at two distinct locations. A healthy child of matching age and gender was also assessed as a control using the same methodology. In all images, areas of affected and unaffected skin were manually selected as regions of

interest (ROI). The mean autofluorescence and diffuse reflectance intensity values within the selected ROIs were analyzed using ImageJ v1.52a software (NIH, Bethesda, MD, USA). Autofluorescence and diffuse reflectance intensity values were calculated based on the Integrated Optical Density (IOD) measurement functionality of the ImageJ software.

Two 4mm punch biopsy samples were obtained from the plantar region of the patient with keratoderma for NLM imaging. One of the biopsy specimens was transferred in phosphate-buffered saline and positioned on slides to capture z-stack images. The second biopsy sample was fixed in formalin, embedded in paraffin, and sliced into 20 μm thick sections. Following deparaffinization, the unstained sections were covered with coverslips for the acquisition of vertical NLM images. To serve as a control, an equivalent set of samples from an unaffected individual underwent identical treatment and processing. For NLM imaging, a sub-ps Ti:Sapphire laser (FemtoRose 300 TUN LC, R&D Ultrafast Lasers Ltd., Budapest, Hungary) with a

repetition rate of approximately 20 MHz was utilized. The imaging system employed was a commercial Axio Examiner LSM 7 MP laser scanning 2P microscope, equipped with a 20 \times , 1.0 NA water immersion objective (W-Plan-APOCHROMAT, Carl Zeiss Microscopy GmbH, Jena, Germany). The pump laser was set to a central wavelength of 800 nm, with a bandwidth of less than 2 nm. A 405/20 nm bandpass filter was employed to collect the SHG signal, while a 590/45 nm (orange) bandpass filter was used for the collection of the TPF signal prior to detection by non-descanned detectors. Two-channel, 16-bit images were acquired from individual imaging areas measuring 420 \times 420 μm^2 , with a pixel dwell time of 12 μs . Mosaic images of vertical skin sections were captured, and the acquired TPF and SHG images were merged and assembled into two-channel images using ImageJ v1.46 software (NIH, Bethesda, MD, USA). Z-stacks of the skin biopsy samples were obtained with a 5 μm step size between horizontal images using Zeiss Zen software v3.0 (Carl Zeiss AG, Germany). Three-dimensional images were generated from these 2D images along the z-axis using ImageJ software.

3.2. Assessment of angiokeratomas in Fabry disease

In this study, we presented findings from a cohort of 26 patients. The diagnosis of FD was established based on reduced alpha-galactosidase A enzyme activity, and genomic DNA sequencing. A comprehensive dermatological examination, including dermoscopic evaluation and photographic documentation, was conducted. Data related to the extracutaneous manifestations of FD were retrospectively collected from clinical records.

We examined dermoscopic images of randomly selected lesions using the Heine Delta 20 dermatoscope (Heine Optotechnik GmbH, Herrsching, Germany). We evaluated specific vascular structures and the presence of the whitish veil.

Different morphologies of angiokeratomas were assessed in our FD patient cohort with MSI. The same setup was used as described earlier. In addition to autofluorescence images under 405 nm illumination and diffuse reflectance images under 526 nm illumination, we

recorded and evaluated diffuse reflectance images under 663 nm and 964 nm illumination.

For NLM investigations, deparaffinized and unstained sections obtained from the angiokeratoma biopsies were prepared. NLM imaging was conducted with the same setup as described earlier, with the following modification, a 525/50 nm (green) bandpass filter was employed to collect the TPF signal. The acquired TPF and SHG images were merged and combined into two-channel images using ImageJ v1.46 software (NIH, Bethesda, MD, USA).

4. RESULTS

4.1. EI case presentation and assesment with MSI and NLM

We presented the case of a 3-year-old male patient with blistering and erosions after birth, followed by the development of erpidermolysis, hyperkaratosis and scaling in the flexural regions. The patient presented palmoplantar kerratoderma as well. Histology showed orthohyperkeratosis and perinuclear vacuolization.

Genetical analysis revealed a heterozygous mutation in the highly conserved region of the *KRT1* gene.

Through quantitative analyses of MSI, it was determined that the palmar hyperkeratosis displayed a notably higher average autofluorescence intensity compared to the clear palmar skin and unaffected skin region of the patient (162.35 vs. 51.14 vs. 20.46). In contrast, the average autofluorescence intensity in the unaffected region of the patient and the healthy control demonstrated a slightly lower value (20.46 vs. 35.97). Concerning the palmar skin, the mean intensity values of the diffuse reflectance images under 526nm excitation were higher in both the patient and control groups (45.83 and 48.12, respectively) when compared to the forearm skin of the patient and control (35.01 and 36.01, respectively). Notably, there was no substantial difference observed in the mean intensity values of the diffuse reflectance imaging between the patient and the healthy control groups.

The visualization of the papillary dermis in the fresh frozen plantar keratoderma sample was hindered due

to the presence of thick hyperkeratosis and strong autofluorescence of keratin. These factors caused significant scattering and resulted in a reduced depth of penetration. The maximum depth reached within the skin was measured at 115 μm for the plantar keratoderma sample and 230 μm for the control sample. For further investigation, mosaic images of vertical skin sections were captured as well. Keratin was visualized with TPF signal, while collagen exhibited SHG signal. In these mosaic images, the dermal papillae could be distinguished with SHG signal, followed by the basal keratinocyte layer that showed TPF signal. Moving upwards, wider cellular layers of the epidermis were observed, accompanied by an increased presence of lamellar structures composed of cornified keratinocytes.

4.2. Assessment of a cohort of FD patients

We assessed the clinical characteristics of 26 FD patients, who presented various extracutaneous signs and symptoms. The most common manifestation of the disease was angiokeratomas in 92% of our patients.

Typically, angiokeratomas in FD present in the bathing suit distribution, between the navel and the thighs. This distribution was observed in eight male and two female patients. We considered it atypical distribution, when a patient presented angiokeratomas on other skin sites, e.g. the upper trunk, arms, which was observed in eleven female and three male patients. We observed papular, warty angiokeratomas as well as incipient, macular angiokeratomas that were either solitary or in clusters. All patients that presented angiokeratomas in the bathing suit distribution had grouped lesions, while most patients presenting angiokeratomas on atypical skin sites e.g. chest, upper extremities almost exclusively presented solitary lesions. Overall, the chest was the most frequent location for angiokeratomas, with a higher prevalence among females. Among males, the umbilical, gluteal, and inguinal regions were the most common sites, which aligns with the bathing suit distribution. We also observed angiokeratomas in acral locations, including the palmoplantar region, ears, and lips.

In regards to other cutaneous signs of FD, 11 patients exhibited an- or hypohydrosis (eight males and three females), and an additional seven patients presented with hyperhidrosis. A majority of our patients displayed various vascular lesions, including teleangiectasias and cherry angiomas. Varicose veins were prevalent in our patient population and could even be observed in young patients. Lymphoedema was also identified in five adult patients. Additionally, synophrys was observed in four young patients, both males and females. Importantly, patients with a low number of angiokeratomas or even those devoid of any angiokeratomas exhibited other cutaneous signs that hold considerable diagnostic value.

A total of 135 dermoscopic images of angiokeratomas were analyzed. Approximately two-thirds of the cases exhibited lacunae, and more than half of the cases manifested as dot-like vessels. Notably, the co-occurrence of lacunae and dot-like vessels was a prevalent observation. Glomerular vessels and linear-irregular structures were identified in around 1/3-1/3 of the cases. The presence of a whitish veil, corresponding to

overlying hyperkeratosis, was detected in only 25% of the cases examined.

Through MSI of angiokeratomas appeared as low-intensity areas on the green (526 nm) and autofluorescent (405 nm) channel. On these channels, the subepidermal vasculature was more discernible, compared to dermoscopy. On the infrared (964 nm) channel, macular angiokeratomas did not exhibit a change in diffuse reflectance signal, while papular angiokeratomas showed reduced diffuse reflectance.

NLM images were captured of an angiokeratoma obtained from our cohort of patients, as well as for a hemangioma serving as a reference for differential diagnosis. The lesions could be differentiated based on morphologic features. In the angiokeratoma sample notable features included a hyperkeratotic surface and dilated capillaries primarily limited to the papillary dermis. In the hemangioma sample, the capillaries extended further towards the subcutaneous tissues. The hemangioma sample was characterized by smaller-diameter vessels that

were separated by thin fibrous septae (visualized with SHG).

5. CONCLUSIONS

We utilized MSI in a case of EI caused by *KRT1* gene mutation. When subjected to 405 nm LED excitation, hyperkeratosis showed a higher autofluorescence response compared to healthy skin.

We used *ex vivo* NLM modalities with particular focus on the visualization of alterations brought on by epidermolytic hyperkeratosis. In case of horizontal imaging with NLM on fresh frozen EI biopsy sample, the presence of thick hyperkeratosis and the strong autofluorescence of keratin posed challenges in visualizing the papillary dermis. The assessment of vertical sections of the EI with NLM provides a detailed label-free imaging of the epidermal layers.

Upon the MSI assessment of angiokeratomas in FD, angiokeratomas can be recognized as areas of reduced intensity compared to the surrounding healthy skin, which is particularly noticeable under 526nm and 405 nm LED illumination. It is worth noting that the subepidermal

blood vessels in the background are more distinguishable, particularly in these channels, in contrast to dermoscopic images. Additionally, upon 964 nm infrared illumination of papular angiokeratomas, the lesions display diminished diffuse reflectance signals. In contrast, macular incipient angiokeratomas do not exhibit reduced diffuse reflectance under the same circumstances, which might be due to the thickness of the lesion.

We assessed an angiokeratoma from a FD patient and a hemangioma from a healthy control with *ex vivo* NLM. We observed significant differences in morphology, the angiokeratoma exhibited hyperkeratosis and ectatic, enlarged blood vessels within the epidermis. In contrast, the hemangioma lacked hyperkeratosis and the vasculature characterized by smaller, proliferative capillaries was not limited to the epidermis and papillary dermis.

Angiokeratomas were present in 92% of our FD patient cohort, which was a considerably higher ratio compared to the literature. We found great clinical heterogeneity regarding the appearance and distribution of angiokeratomas in our FD patient cohort. In the bathing

suit distribution the angiokeratomas formed clusters, which was mainly seen in males, while female patients were more likely to present solitary angiokeratomas on the trunk and extremities. Warty, papular as well as macular or incipient angiokeratomas could be observed regardless of age and gender. Only 38% of the patients, mainly males, presented the typical form of ACDU in the bathing suit distribution. While the majority of individuals in our group of patients presented angiokeratomas in an atypical distribution or appearance.

Dermoscopy can have a notable benefit in the assessment of incipient angiokeratomas. While dermoscopic images of angiokeratomas also showed great variability. Angiokeratomas primarily showed the presence of dark red lacunae, often accompanied by dot-like vascular structure. The whitish veil corresponding to hyperkeratosis was only observed in 25% of our cases.

6. LIST OF PUBLICATIONS

Publications related to the thesis

Anker P. Fésűs L, Kiss N, Noll J, Becker K, Kuroli E, Mayer B, Bozsányi S, Lőrincz K, Lihacova I, Lihachev A, Lange M, Wikonkál N, Medvecz M. Visualization of Keratin with Diffuse Reflectance and Autofluorescence Imaging and Nonlinear Optical Microscopy in a Rare Keratinopathic Ichthyosis. *Sensors* (Basel). 2021;21(4):1105. (IF: 3,847)

Anker P. Fésűs L, Kiss N, Lengyel A, Pinti É, Lihacova I, Lihachev A, Plorina EV, Fekete G, Medvecz M. A Cross-Sectional Study of the Dermatological Manifestations of Patients with Fabry Disease and the Assessment of Angiokeratomas with Multimodal Imaging. *Diagnostics* (Basel). 2023;13(14):2368. (IF: 3,6)

Publications not related to the thesis

Kiss N, **Anker P.** Fésűs L, Lőrincz K, Bánvölgyi A, Bozsányi S, Wikonkál N. A rosszindulatú hámeredetű bőrdaganatok kialakulásának genetikai háttere, új ismeretek a karcinogenezis folyamatában. *Börgy Vener Szeml.* 2018; 94:5 pp. 220-226.

Bánvölgyi A, **Anker P.** Lőrincz K, Kiss N, Márton D, Fésűs L, Gyöngyösi N, Wikonkál N. Smoothened receptor inhibitor vismodegib for the treatment of basal cell carcinoma: a retrospective analysis

of efficacy and side effects. *J Dermatol Treat.* 2020; 31(4):387- 398. (IF: 3,359)

Kiss N, **Anker P**, Bánvölgyi A, Lőrincz, Fésűs L, Bozsányi S, Szipőcs R, Medvecz M, Wikonkál N. Új képpalkotó technikák a bőrgyógyászatban és azok klinikai alkalmazása. *Bőrgy Vener Szeml.* 2019; 95(3): 90-99.

Bánvölgyi A, **Anker P**, Kiss N, Lőrincz K, Wikonkál N, Medvecz M. Gyulladásos bélbetegségek bőrgyógyászati vonatkozásai – a bél-mikrobiom tükrében. *Gasztroent Hep Szeml.* 2019; 5(2): 3-7.

Anker P, Medvecz M. Ichthyosisok patogenezise: a terminális differenciáció zavarai. *Bőrgy Vener Szeml.* 2020; 96(1): 3-10.

Farkas K, Bozsányi S, Plázár D, Bánvölgyi A, Fésűs L, **Anker P**, Zakariás S, Lihacova I, Lihachev A, Lange M, Arányi T, Wikonkál NM, Medvecz M, Kiss N. Autofluorescence Imaging of the Skin Is an Objective Non-Invasive Technique for Diagnosing Pseudoxanthoma Elasticum. *Diagnostics.* 2021; 11(2):260. (IF: 3,992)

Bozsányi S, Farkas K, Bánvölgyi A, Lőrincz K, Fésűs L, **Anker P**, Zakariás S, Jobbágy A, Lihacova I, Lihachev A, Lange M, Bliznuks D, Medvecz M, Kiss N, Wikonkál NM. Quantitative Multispectral Imaging Differentiates Melanoma from Seborrheic Keratosis. *Diagnostics (Basel).* 2021;11(8):1315. (IF: 3,992)

Haász C, Kuroli E, **Anker P**, Márton DF, Szigeti Á, Nagy Z, Demeter J, Sárdy M, Medvecz M. Periorbitalis

bőrtünetekkel járó könnyűlanc-amyloidosis. Orv Hetil. 2021; 162 (32). pp. 1303-1308. (IF: 0,707)

Anker P, Kiss N, Kocsis I, Czemmel É, Becker K, Zakariás S, Plázár D, Farkas K, Mayer B, Nagy N, Széll M, Ács N, Szalai Z, Medvecz M. Report of a Novel ALOX12B Mutation in Self-Improving Collodion Ichthyosis with an Overview of the Genetic Background of the Collodion Baby Phenotype. Life (Basel). 2021;11(7):624. (IF: 3,253)

Pála S, **Anker P**, Farkas K, Plázár D, Kiss S, Marschalkó P, Szalai Z, Bene J, Hadzsiev K, Maróti Z, Kalmár T, Medvecz M. Co-occurrence of neurofibromatosis type 1 and pseudoachondroplasia - a first case report. BMC Pediatr. 2023 Mar 8;23(1):110. (IF: 2,4)